Nano Energy 41 (2017) 749–757

Contents lists available at ScienceDirect

Nano Energy

journal homepage: www.elsevier.com/locate/nanoen

Full paper

Molybdenum carbide on hierarchical porous carbon synthesized from Cu-MoO_2 as efficient electrocatalysts for electrochemical hydrogen generation

Jin Jia[a], Weijia Zhou[a,*], Zhaoqian Wei[a], Tanli Xiong[a], Guixiang Li[a], Lili Zhao[b], Xiaofei Zhang[b], Hong Liu[b], Jian Zhou[c], Shaowei Chen[a,d,**]

[a] Guangzhou Key Laboratory for Surface Chemistry of Energy Materials, New Energy Research Institute, School of Environment and Energy, South China University of Technology, Guangzhou Higher Education Mega Center, Guangzhou, Guangdong 510006, PR China
[b] State Key Laboratory of Crystal Materials, Center of Bio & Micro/Nano Functional Materials, Shandong University, 27 Shandanan Road, Jinan, Shandong 250100, PR China
[c] National Laboratory of Solid State Microstructures and Department of Materials Science and Engineering, Nanjing University, 22 Hankou Road, Nanjing, Jiangsu 210093, PR China
[d] Department of Chemistry and Biochemistry, University of California, 1156 High Street, Santa Cruz, CA 95064, USA

ARTICLE INFO

Keywords:
Molybdenum carbide
Porous carbon rod
Cu template
Catalytic site
Hydrogen evolution reaction

ABSTRACT

Hydrogen evolution reaction (HER) from water electrolysis, currently, is fundamental for large-scale solar fuel production by utilizing earth-abundant element and non-noble metal-based catalysts. Herein, Mo_2C on hierarchical porous carbon rods composed of cross-linked carbon networks (Mo_2C/CLCN) was synthesized by using Cu-MoO_2 rods as Mo source and Cu template. The copper plays key roles in protecting Mo_2C from excess covering carbon to enhance the HER performance. When evaluated for HER activity, Mo_2C/CLCN exhibit a low onset potential of −85 mV with a Tafel slope of 48.2 mV dec^{-1}, an operating overpotential of 145 mV at the cathodic current density of 10 mA cm^{-2} and outstanding long-term cycling stability in acidic electrolyte, which superior to most of non-doping Mo_2C. This work suggests that the in-situ template method by multi-element compounds is an inspiring strategy for synthesizing the efficient water splitting electrocatalysts with high electrochemical active area and more catalytically active sites.

1. Introduction

Currently, the surge in the field of renewable energy targeting to exploit clean energy technology is ongoing to upsurge [1–4]. To satisfy the twofold challenges of fossil fuel exhaustion and global greenhouse emission, so hydrogen has been proved to be one of the advantaged candidates for an eco-friendly and even renewable energy carrier. Hydrogen evolution reaction (HER) is receipting increasing public attentions in virtue of water electrolysis, which requires high-performance electrocatalysts. Although Pt-based and other noble metal catalysts are competent HER catalysts possessing high production efficiency at low overpotential, the scarcity and expensiveness of them impede their widespread industrialization applications [5–8]. Therefore, research focus has been shifted to precious-metal-free based materials for an efficient HER [2,9–12]. Transition metal carbides (Mo_2C [13,14], WC [15], and TaC [5] etc.) have been recognized as low cost catalyst alternatives for HER reaction because of their earth-abundant composition and highly catalytic activity.

Particularly, molybdenum carbide (Mo_2C) has been suggested to be a capable substitution of Pt-based electrocatalysts for water electrolysis owing to its electronic structure is analogous to that of Pt metal [16,17]. The catalytic performance of Mo_2C for HER primarily relies on the exposed Mo catalytic site numbers, conductivity and efficient active surface. Researchers have given a demonstration that the electrocatalytic activity of HER may perhaps be improved by means of structuring appropriate Mo_2C nanostructures, such as nanoporous Mo_2C nanowires [18], Mo_2C nanocrystallites [19], and hierarchical Mo_2C nanotubes [20]. Prof. Lou et al. [13] reported a novel copper-based metal-organic frameworks-assisted approach for constructing nanostructured MoC_x nano-octahedrons as an exceedingly efficient electrocatalyst for water splitting. Prof. Zou et al. [21] reported a simple preparation process of the ultra-small Mo_2C nanoparticles implanted within plentiful nitrogen-doped carbon nanolayers (Mo_2C@NC), which possess the noteworthy HER activity and excessive robustness at all-pH

* Corresponding author.
** Corresponding author at: Guangzhou Key Laboratory for Surface Chemistry of Energy Materials, New Energy Research Institute, School of Environment and Energy, South China University of Technology, Guangzhou Higher Education Mega Center, Guangzhou, Guangdong 510006, PR China.
E-mail addresses: eszhouwj@scut.edu.cn (J. Zhou), shaowei@ucsc.edu (S. Chen).

http://dx.doi.org/10.1016/j.nanoen.2017.10.030
Received 3 July 2017; Received in revised form 28 July 2017; Accepted 12 October 2017
Available online 14 October 2017

of 0–14. Nevertheless, it is still greatly eager for innovative efficient methods to synthesize pure Mo_2C catalysts with high HER activity and eliminate the influence of the nonmetal doping.

Hu and his colleagues [22] speculated that Mo atoms of Mo_2C may behave just like noble metals, and serve on the active sites for HER. Therefore, how to expose more Mo active sites is an important strategy of enhancing the catalytic activity of Mo_2C. All kinds of carbon sources, such as CH_4 [23], glucose [24], dicyandiamide [21,25], aniline [18,26] and dopamine [27] were used to synthesize Mo_2C. In the usual synthesis process, the nonmetal elements doping, such as N atoms from nitrogen-containing compounds [18,21,25–27], can regulate electronic state density of carbon to enhance the HER activity of Mo_2C. However, phase-pure Mo_2C synthesized by pure carbon sources, such as CH_4 and glucose, usually possessed the poor HER activity [18], because the residual carbon may risk extensive coking of Mo active sites [28]. Prof. Roman-Leshkov reported that the silica-encapsulated tungsten oxide nanoparticles were carburized by CH_4/H_2, then removed silica protective cover to synthesize metal-terminated tungsten carbide (WC) nanoparticles. The silica protective cover can avoid surface impurity deposition to expose W active sites during carbonation process, which possessed the activities about 100-fold higher than commercial WC and within an order of magnitude of platinum based catalysts for HER [29].

Herein, we developed a novel process of self-template to grow Mo_2C on hierarchical porous rods composed of cross-linked carbon network (Mo_2C/CLCN). In which, Cu-MoO_2 were used as Mo source and Cu template and CH_4 was used as pure carbon source to synthesize phase-pure Mo_2C. The copper plays key roles in the formation of hierarchical porous carbon to increase electrochemical active area and exposure of Mo_2C without excessive surface carbon to enhance the HER activity. Mo_2C/CLCN without nonmetal doping exhibited efficient HER electrocatalytic activity with a small onset potential of −85 mV, a Tafel slope of 48.2 mV dec^{-1} in acidic electrolyte and outstanding long-term cycling stability in broad pH range.

2. Experimental

2.1. Chemicals and materials

The analytical grade of ammonium molybdate ($(NH_4)_6Mo_7O_{24}{\cdot}4H_2O$), copper(II) chloride dihydrate ($CuCl_2{\cdot}2H_2O$) and 20 wt% Pt/C, were purchased from Sinopharm Chemical Reagents Beijing Co., and Nafion solution (~ 5% in a mixture of lower aliphatic alcohols and water) were purchased from SIGMA-ALDRICH Shanghai Co. Mixed gases of argon and hydrogen (H_2-Ar, 10 vol% H_2) and methane (CH_4) were obtained from Guangzhou YIGAS Gases CO., LTD.

2.2. Synthesis of Cu-MoO_2 rods

$CuCl_2{\cdot}2H_2O$ (1.4 mmol) in 40 mL deionized water and $(NH_4)_6Mo_7O_{24}{\cdot}4H_2O$ (1 mmol) in 40 mL deionized water were mixed by magnetic stirring for 3 h. After drying, the obtained green precursor was placed at the center of the quartz tube (length: 50 cm and diameter: 5 cm) inside a tubular furnace. Subsequently, the mixture was heated from room temperature to 450 °C with a heating rate of 5 °C/min and was maintained at 450 °C for 4 h under an Ar-H_2 (10%) mixture gas flow of 50 sccm. After the calcination, the black Cu-MoO_2 rods were obtained. Except for special instructions, the Cu-MoO_2 rods were synthesized with molar ratio between Cu and Mo (1:5). In addition, the high molar ratio of Cu/Mo (1:1) was employed to synthesize Cu-MoO_2 rods to study the effect of structural regulation by Cu.

2.3. Synthesis of Mo_2C on hierarchical porous rods composed of cross-linked carbon network (Mo_2C/CLCN)

The Cu-MoO_2 rods in a ceramic crucible were placed in the tube furnace, heated up to 1000 °C under Ar (10 sccm) atmosphere. Once the 1000 °C reached, the Ar was shut off and CH_4 (400 sccm) was introduced into the tube for 8 min. Finally, the tube furnace was cooled to room temperature naturally under Ar. The as-made material was denominated as Cu-Mo_2C/CLCN rods. The Cu was etched by 0.01 M $FeCl_3$ aqueous solution for 80 min to obtain Mo_2C/CLCN, which were separated by filtration, washed repeatedly and then desiccated by the vacuum freeze-drying. The effect of etching time by 0.01 M $FeCl_3$ (10 min, 40 min, 80 min and 120 min) and 3 M $FeCl_3$ aqueous solution combined with ultrasonic treatment (80 min) on HER performance of Mo_2C/CLCN was also studied.

The blank samples of Mo_2C-S1 and Mo_2C-S2 were synthesized as followed. In order to study the rod structure and HER activity of Mo_2C/CLCN regulated by Cu, the Mo_2C-S1 was synthesized by using $(NH_4)_6Mo_7O_{24}{\cdot}4H_2O$ powders first reduced by Ar/H_2 (50 sccm) at 450 °C for 4 h and then carbonized by CH_4 (400 sccm) at 1000 °C for 8 min in a quartz tube furnace, which was prepared following the same calcining procedure as Mo_2C/CLCN. In order to study the Cu protective effect of Mo catalytic sites in Mo_2C/CLCN, the Mo_2C-S2 was synthesized. The porous MoO_2 rods obtained by removing Cu of Cu-MoO_2 rods by 0.01 M $FeCl_3$ was used as Mo precursor, then carbonized by CH_4 (400 sccm) for 8 min at 1000 °C in a quartz tube furnace.

2.4. Characterization

Phase compositions of the as-made materials were measured by D8 Advance (Germany Bruker) X-ray diffractometer (XRD) with Cu Kα radiation (λ = 0.15406 nm). Raman spectra were obtained by a LabRAM HR800 spectrometer (Horiba Jobin Yvon, FR.) equipped with an Ar laser (wavelength = 514.5 nm) and a long working distance 50 × objective lens. Morphologies of the materials were identified by a field emission scanning electron microscope (FESEM, MERLIN Compact, Carl Zeiss) and a transmission electron microscope (TEM, a JEM-2100F Field Emission Electron Microscope, JPN) at an acceleration voltage of 200 kV. The two kinds of Mo_2C/CLCN, including entire rod and fragment from Mo_2C/CLCN obtained by common and super ultrasonic processing, respectively, were characterized by TEM. X-ray photoelectron spectroscopic (XPS) measurement was performed using a PHI X-tool instrument (Ulvac-Phi). Brunauer-Emmett-Teller (BET) specific surface area (SSA) and pore size distribution (PSD) were obtained by using a Quantachrome Autosorb-IQ_2 instrument with nitrogen adsorption at 77 K using the Barrett-Joyner-Halenda (BJH) method.

2.5. Electrochemical measurements

Electrochemical measurements were performed with an electrochemical workstation (CHI 760E, Chenhua Instruments Inc.) in 0.5 M H_2SO_4. An Hg/Hg_2Cl_2 electrode (SCE, saturated KCl) and carbon rod were used as the reference and counter electrode, separately. 5 mg sample was dispersed in 1 mL of 4:1 (v: v) water/ethanol mixed solvents along with 50 μL Nafion solution, and the mixture was sonicated enough. Then, 5 μL mixture was dripped over the glassy-carbon electrode of 0.07 cm^2 at a catalyst loading of 0.357 mg cm^{-2}. Polarization curves were achieved by sweeping the potential from 0 to −0.5 V vs. RHE at a sweep rate of 5 mV s^{-1} in 0.5 M H_2SO_4 (pH 0.25), 1 M phosphate buffer (pH 7) and 1 M KOH (pH 14), which were used as electrolytes. Unless specifically mentioned, all the electrochemical measurements were iR-uncorrected. AC impedance was detected with a frequency range and an amplitude of 5 mV from 0.01 Hz to 100 kHz. The main arc in electrochemical impedance spectroscopy (EIS) spectra was matched utilizing a simplified Randles equivalent circuit, which was comprised of a resistance (Rs) in series with a parallel arrangement of a charge-transfer resistance (Rct) and a constant phase element (CPE), and the fitting parameters were appraised through the Levenberg-Marquardt minimization procedure. Cyclic voltammetry (CV) was applied to measure the electrochemical double layer

capacitance at nonfaradaic potentials as another way to reckon the efficient electrochemical active area of HER. Current-time responses were detected for 12 h by chronoamperometric measurements. Gas chromatographic measurements (GC-2060F, LuNan Analytical Instruments, LTD, China) were employed to quantify the amount of hydrogen gas production.

2.6. DFT calculation

The calculations were performed using the density functional theory (DFT) as implemented in the Vienna Ab Initio Simulation Package (VASP) [30,31], the projector augmented wave method and the PBE exchange-correlation function were used [32,33]. A 4 × 4 × 1 molybdenum carbide supercell with a vacuum layer of 15 Å was constructed and then cleave the (001) facet to simulate the surface of Mo_2C. The Brillouin zone integration was performed on a Γ-center 5 × 5 × 1 k-point mesh, and the Gaussian smearing width was 0.05 eV. The cutoff energy was 520 eV during the calculation. The atomic positions were fully optimized until the maximum residual forces of all of the atoms were less than 0.02 eV $Å^{-1}$. The Gibbs free energy of hydrogen absorption (ΔG_H) was calculated as follows: $\Delta G_H = \Delta E_H + 0.24$ eV, where $\Delta E_H = E_{M+H} - E_M - 1/2E_{H_2}$ (E_{M+H} is the total energy of the Mo_2C surface with a single hydrogen atom absorbed on the surface, E_M is the total energy of the Mo_2C surface, and E_{H_2} is the total energy of a hydrogen molecule in the gas phase) [34].

3. Results and discussion

Based on prior structural data, Mo_2C can be described as a hexagonal-close-packed layer of Mo atoms, with C atoms randomly filling half of the octahedral interstitial sites. A supercell (4 × 4 × 1) of molybdenum carbide with (001) plane was constructed. DFT calculations were used to calculate the Gibbs free energy of H* adsorption (ΔG_{H^*}) of Mo atoms and C atoms on different sites of Mo_2C. Mo-1 and Mo-2 atoms of Mo_2C possessed the smaller $|\Delta G_{H^*}|$ values of 0.03 eV and 0.06 eV, respectively, which were much lower than that of C-1 atom (0.45 eV), implying that Mo atoms on C plane are the main catalytic sites of Mo_2C (Scheme 1**a**). Usually, the residual carbon atoms during carbonation process saturated the surface of as-obtained Mo_2C (inset of Scheme 1**b**), which covered Mo catalytic sites, only remained the inert carbon atoms of C-1 (−0.46 eV) and C-2 (−0.8 eV). Thus, how to expose the catalytic active Mo sites of Mo_2C is the important research content.

Herein, we reported a self-template of Cu-MoO_2 rods as Mo source and Cu template, followed by the Cu etching process, to grow Mo_2C/CLCN. The transformation of structural models and schematic illustration of the detailed synthetic procedure for Mo_2C/CLCN were shown in Scheme 2. When carbonization reaction occurred, the Mo_2C and graphene sheets on Cu were synthesized, respectively. The Cu atoms protected Mo_2C from being covered by excessive carbon. After removing the Cu, the Mo_2C were exposed and CLCN was obtained. The detailed synthetic procedure for Mo_2C/CLCN was listed as follow. Step (a), Cu-MoO_2 rods were synthesized at 450 °C by reducing the Cu-Mo precursors (Cu/Mo = 1:5) with Ar-H_2 (10%) mixture gas and the existence of Cu played a crucial role in forming Cu-MoO_2 rods. However, the too much copper (Cu/Mo = 1:1) will melt out from Cu-MoO_2 rods and form Cu nanoparticles on the surface of rods (Fig. S1). Step (b), Cu-MoO_2 rods were transformed into Cu-Mo_2C/CLCN by carbonizing reaction via CH_4 as carbon source. During the process, the MoO_2 was transformed into Mo_2C. Meanwhile, the carbon sheets catalytically synthesized on the surface of Cu. Step (c), the Cu was removed by 0.01 M $FeCl_3$ via redox reaction ($2Fe^{3+} + Cu = Cu^{2+} + 2Fe^{2+}$) and then the Mo_2C were exposed, which enhanced the HER activity.

To confirm the formation process of Mo_2C/CLCN, the field emission scanning electron microscope (FESEM) (Fig. 1), X-ray diffractometer (XRD) (Fig. 2**a**), Raman (Fig. 2**b**) and X-ray photoelectron spectroscopy (XPS) (Fig. 2**c and d**) analyses were used to monitor the morphological and structural evolution as a function of the reaction process. The Cu-MoO_2 rods were synthesized in an Ar-H_2 atmosphere at 450 °C for 4 h. As shown in Fig. 1**a**, the well-crystalline Cu-MoO_2 microrods with a smooth surface possessed an average diameter of ~ 2 μm and length of 5–6 μm. After the carbonizing reaction, Cu-MoO_2 rods were transformed into Cu-Mo_2C/CLCN. The rod-shaped morphology was retained, but the coarse carbon layers on the surface of rods were observed (Fig. 1**b**). In this process, the Cu not only catalytically synthesized porous carbon but also protected Mo_2C from covering excessive carbon. Eventually, Mo_2C/CLCN were produced by dissolution of Cu in 0.01 M $FeCl_3$ solution. After removing Cu, the rod structure was remained and plentiful pores were produced in the meanwhile (Fig. S2, Fig. 1**c and d**). The walls of the claviform structure were randomly constructed by the connective graphene-like ultrathin nanosheets.

Energy dispersive spectrometer (EDS) mapping of Cu, Mo and C was used to characterize the changed element composition of synthetic process. The main components of Cu, Mo, O and the noise signals of carbon were detected in Cu-MoO_2 with evenly distributed rods (Fig. 1**e**). After carbonation, main elements of Mo, Cu and C were the main components of Mo_2C/CLCN (Fig. 1**f**). After the etching process, Cu element was not detected, implying the successful removal of Cu (Fig. 1**g**). The element percentages of Cu, Mo and C in Cu-MoO_2, Cu-Mo_2C/CLCN and Mo_2C/CLCN were summarized in Fig. 1**h** and Table S1.

During the reaction, the phase transformations from Cu-MoO_2 to Cu-Mo_2C/CLCN, then to Mo_2C/CLCN were confirmed by XRD measurements (Fig. 2**a**). As for Cu-MoO_2, the main characteristic diffraction peaks of MoO_2 were observed at 26°, 36.98°, 41.62°, 53.46°, 60.32°, 66.5° attributable to the crystal faces of (011), (211), (210), (311),

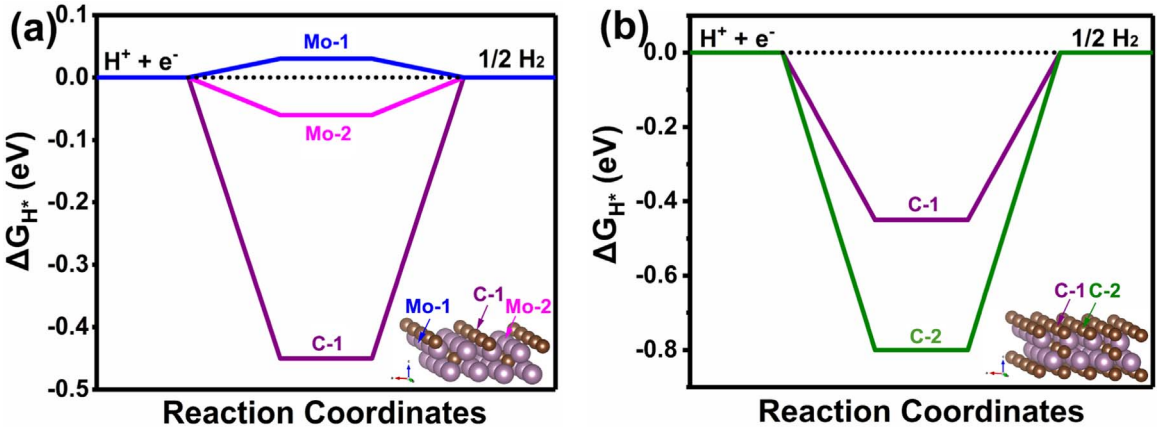

Scheme 1. Gibbs free energy of H* adsorption of (a) theoretical Mo_2C and (b) Mo_2C with the saturated carbon atoms. Inset are the according structural models and calculated sites.

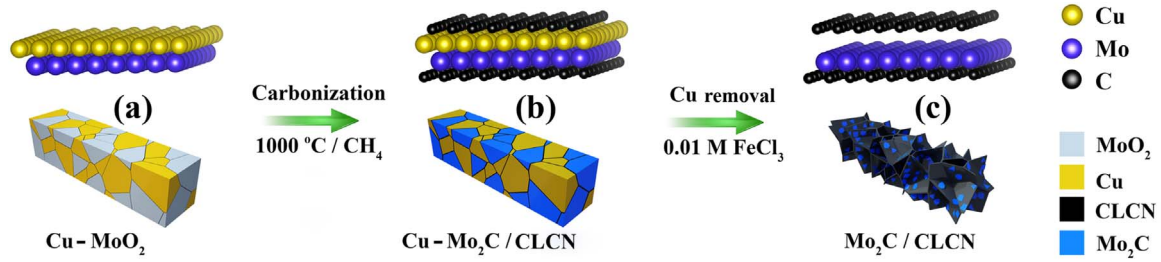

Scheme 2. Structural models and schematic illustration of the synthetic procedure for Mo_2C/CLCN.

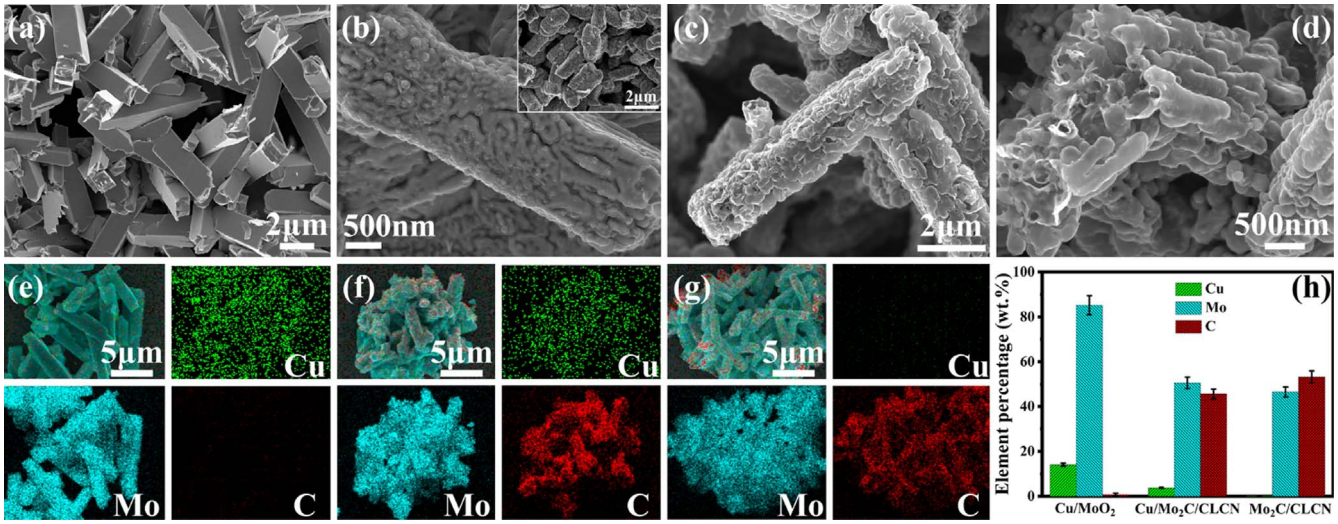

Fig. 1. SEM images and according C, Mo and Cu elements mapping of (a, e) Cu-MoO_2; (b, f) Cu-Mo_2C/CLCN; (c, d, g) Mo_2C/CLCN; (h) element percentage of Cu-MoO_2, Cu-Mo_2C/CLCN and Mo_2C/CLCN.

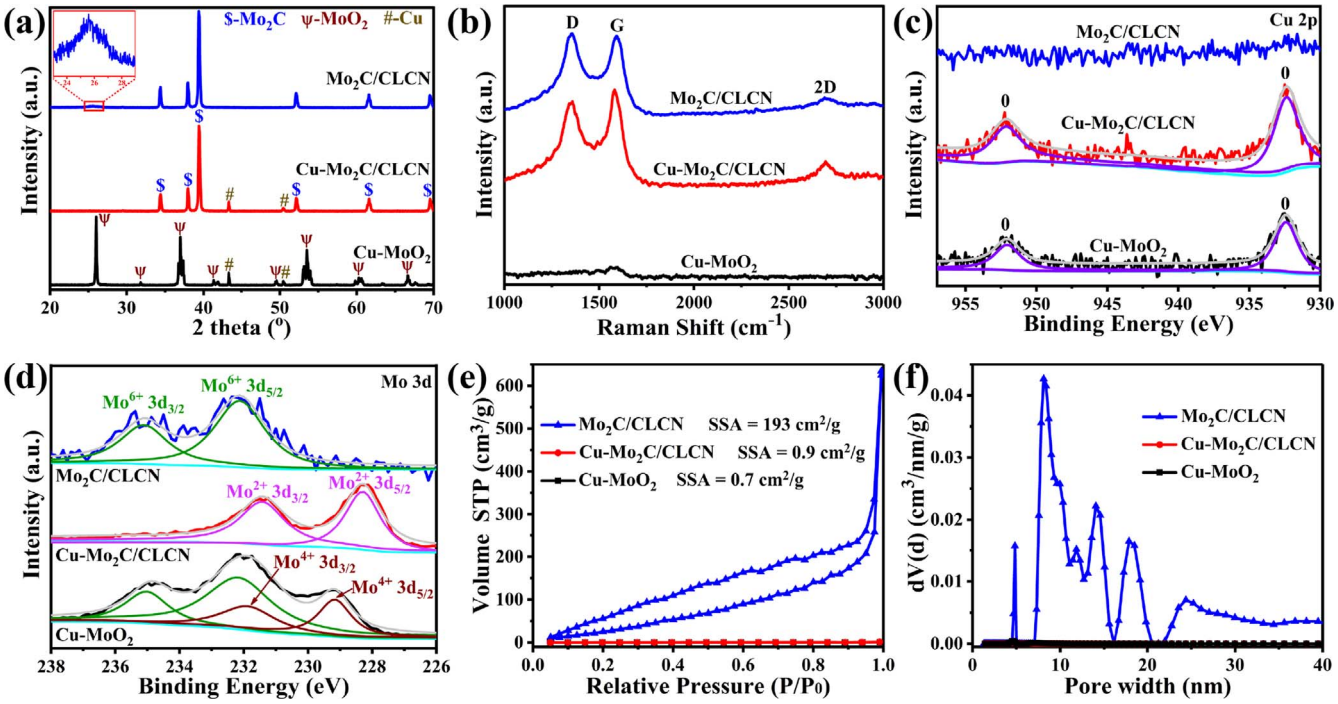

Fig. 2. (a) XRD patterns; (b) Raman spectra; XPS spectra of (c) Cu 2p and (d) Mo 3d; (e) N_2 adsorption-desorption isotherms and (f) the corresponding pore size distributions of Cu-MoO_2, Cu-Mo_2C/CLCN, and Mo_2C/CLCN.

(013), (402) (PDF# 78-1069). Additionally, the weak diffraction peaks of cubic Cu (PDF# 85-1326) were detected at 43.3° and 50.5°, indicating the coexistence of Cu and MoO_2 in Cu-MoO_2 rods. After carbonization treatment, the diffraction peaks of Cu still existed, but the MoO_2 were fully transformed into the β-Mo_2C with the according diffraction peaks at 34.4°, 38.0°, 39.4°, 52.1°, 61.5°, and 69.6°

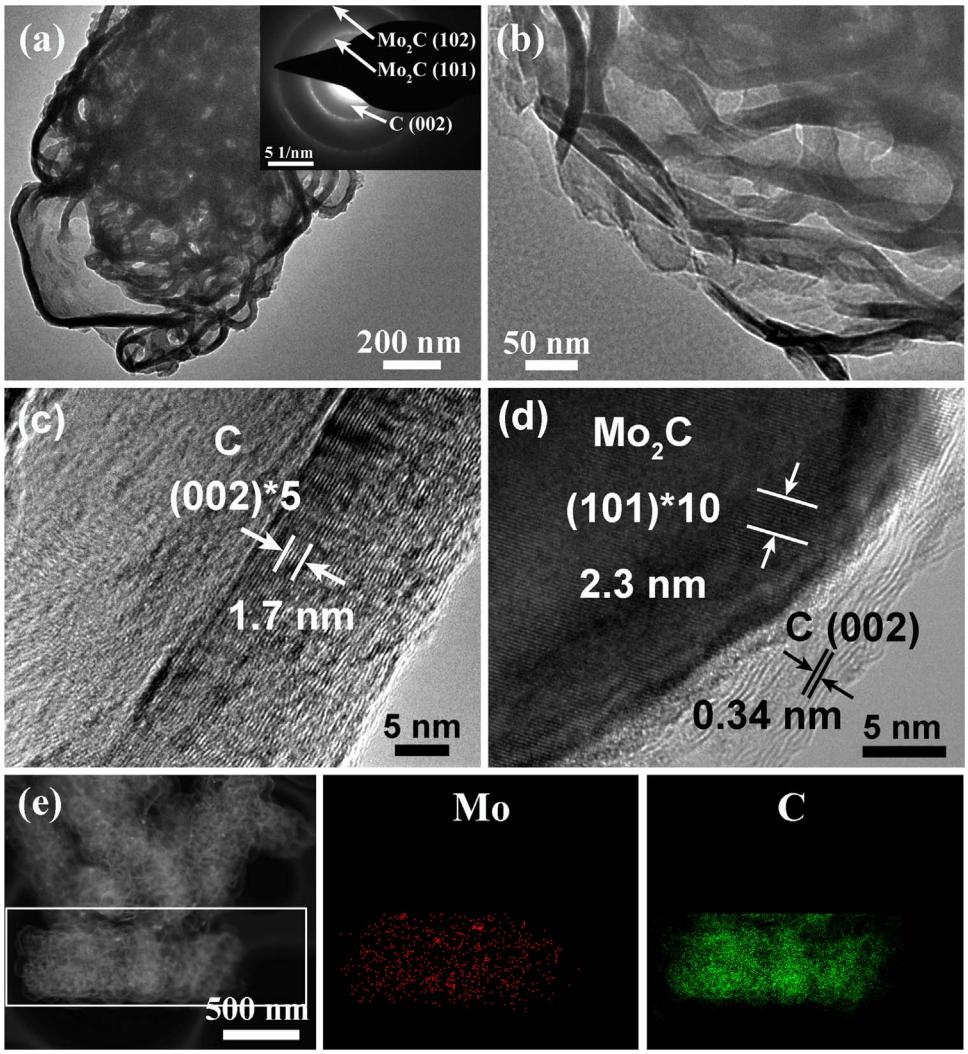

Fig. 3. (a-c) (HR)TEM images of Mo_2C/CLCN, inset of (a) is electron diffraction pattern of Mo_2C/CLCN; (d) HRTEM image of the fragment from Mo_2C/CLCN by crushing processing; (e) Mo and C element mappings of Mo_2C/CLCN.

corresponding well to the crystal planes of (100), (002), (101), (102), (110) and (103) (β-Mo_2C, PDF# 35-0787). After etching treatment by $FeCl_3$, the diffraction peaks of Cu disappeared, and only main β-Mo_2C was remained. In addition, the weak diffraction peak at ~ 26° of crystalline carbon was detected as shown in inset of Fig. 2**a**. The Raman spectra also confirmed the similar transformation process as shown in Fig. 2**b**. After carbonation, the characteristic peaks of defective carbon (D peak, at 1356 cm^{-1}) and crystalline carbon (G peak, at 1583 cm^{-1}) appeared. In addition, after etching treatment, the ratio of I_D/I_G increased from 0.55 to 0.59, suggesting the introduction of more defects in Mo_2C/CLCN. These samples were further analyzed by XPS. As shown in Fig. 2**c**, the Cu^0 were detected in Cu-MoO_2 with the characteristic Cu 2p of spectra at ~ 932 eV and ~ 952 eV. After carbonization, only Cu^0 was still detected possibly due to the further reduction reaction of carbon and nonexistence of oxidation state in Cu-Mo_2C/CLCN. After etching treatment, no Cu was detected in Mo_2C/CLCN, implying the Cu as template was removed. In addition, as shown in Fig. 2**d**, the peak fitting of Mo 3d at 235 eV, 232 eV, 232 eV and 229 eV suggested the +6 and +4 states of Mo in Cu-MoO_2 [35,36]. After carbonization, the main Mo^{2+} with peaks at 231 eV and 228 eV (Mo $3d_{5/2}$ and Mo $3d_{3/2}$) were observed in Cu-Mo_2C/CLCN. The following etching treatment, the oxidation states (Mo^{6+} species) were detected on the surface of Mo_2C/CLCN due to the oxidation of $FeCl_3$, which are commonly observed on the surface of molybdenum carbide exposed to air [18,22,37,38]. A trace of Mo^{6+} species on the surface of Mo_2C/CLCN did not affect the HER activity, which was confirmed in Fig. S3. No residual Fe were detected in Mo_2C/CLCN after full washing by deionized water (Fig. S4).

In order to study the pore-creating effect of Cu, the Brunauer-Emmett-Teller (BET) method was applied to measure the BET surface area and porous structure. Fig. 2**e** displayed the N_2 adsorption-desorption isotherms of Cu-MoO_2, Cu-Mo_2C/CLCN and Mo_2C/CLCN, which showed the according BET specific surface areas of 0.7 $m^2\ g^{-1}$, 0.9 $m^2\ g^{-1}$ and 193 $m^2\ g^{-1}$, respectively. Mo_2C/CLCN can be categorized as a typical II isotherm with the hysteresis loop (belong to type H3), which indicated the existence of mesoporous network structure. It was drawn attention that the uptrend of isotherm terminal was connected with the isotherms of plate-like materials due to the increasing aggregates of macropores or slit-shaped pores. Besides, the pore volume of 0.97 $cm^3\ g^{-1}$ with the pore size distribution of 5–30 nm in Mo_2C/CLCN was measured, but no porous structure was observed in Cu-MoO_2 and Cu-Mo_2C/CLCN as shown in Fig. 2**f**. The results confirmed that the Cu played an important role in forming the porous structure of CLCN. In order to discuss the effect of Cu on the morphological control and formation of CLCN, some blank samples were synthesized. Sample 1 of Mo_2C (Mo_2C-S1) was synthesized by similar process without Cu. XRD results in Fig. S5a confirmed the successful synthesis of Mo_2C with same crystal phase. SEM image of Mo_2C-S1 showed the numerous thick Mo_2C plates instead of Mo_2C rods, demonstrating that the existence of Cu can regulate the synthesis of rod structure (Fig. S5b). Furthermore, before carbonizing reaction, the porous MoO_2 rods (Figs. S6 and S7) synthesized by removing Cu from Cu-MoO_2 were used to synthesize Mo_2C porous rods, which were labeled as Sample 2 (Mo_2C-S2). SEM image

(Fig. S8a) and XRD (Fig. S8b) result displayed the porous rods were constituted of the numerous Mo_2C particles. However, the BET surface area of Mo_2C-S2 was significantly decreased, which was only 14.2 $m^2 g^{-1}$ as shown in Fig. S8c, demonstrating that the existence of Cu regulated the synthesis of CLCN with high surface area [39]. May safely draw the conclusion that, because the existence of copper, Cu-MoO_2 not only acts as the regulating agent of rod morphology but also provides the template for the preparation of CLCN.

The structural transformation and the highly porous texture throughout the cross-section of Mo_2C/CLCN were characterized by transmission electron microscopy (TEM). The single-crystal structure of Cu-MoO_2 rod possessed the lattice spacing of 0.34 nm corresponding to the (011) plane of MoO_2 (Fig. S9a). A lot of defect areas were observed in rod possibly due to the existence of Cu. However, no obvious Cu nanoparticles were detected in rod possibly due to the small particle size. At last, the EDX mapping of single Cu-MoO_2 rod confirmed that the Mo and Cu elements were evenly distributed in rod (Fig. S9b). After carbonization, Cu-Mo_2C/CLCN possessed the solid rod structure with carbon layer, as shown in Fig. S10. After removing of Cu to form Mo_2C/CLCN, the porous rods were consisted of the graphene-like nanosheets with the thickness of 5–20 nm were observed (Fig. 3**a and b**). A representative high-resolution TEM (HRTEM) image clearly showed the lattice fringes with the interplanar spacing of 0.34 nm on the edge, corresponding to the (002) planes in the broadside of carbon sheet (Fig. 3**c**). Curiously, no obvious Mo_2C nanoparticles were observed on the surface of CLCN. However, the selected-area electron diffraction (SAED) pattern of Mo_2C/CLCN confirmed the polycrystalline nature with multiple-unit of diffraction rings, which was composed of (002) of carbon and (101), (102) of Mo_2C, as shown in inset of Fig. 3**a**. In addition, SEM (Fig. 1), XRD (Fig. 2**a**) and XPS (Fig. 2**d**) results also confirmed the existence of abundant and high crystalline Mo_2C. According to synthetic procedure in Scheme 2, the synthesized Mo_2C was loaded on the internal surface of CLCN. In order to confirm the speculation, the Mo_2C/CLCN rods were broken by super ultrasonic processing to obtain the fragments (Fig. S11). As expected, a large area of lattice fringes with the interplanar spacing of 0.23 nm (Fig. 3**d**), matching with the (101) plane of Mo_2C were observed on the surface of carbon sheets. In similar reported result, Cu foil as catalyst substrate fabricated large-area 2D ultrathin Mo_2C sheets [22]. At last, EDX-mappings further confirmed that the uniform distributions of Mo and C of Mo_2C/CLCN in rod structure (Fig. 3**e**). Therefore, the multilevel structures of Mo_2C/CLCN rods were visually splited into two parts: 3D porous rods composed of the cross-linked carbon nanosheets and Mo_2C nanoparticles on the internal surface of carbon nanosheets.

The electrocatalytic HER activities of Mo_2C/CLCN along with Cu-MoO_2, Cu-Mo_2C/CLCN, Mo_2C-S1, Mo_2C-S2 and commercial 20 wt% Pt/C were investigated in 0.5 M H_2SO_4 solution by employing a typical three-electrode setup. The HER polarization curves in Fig. 4**a** showed that Mo_2C/CLCN have the lowest onset potential (η_0) of −85 mV vs. RHE (achieve 1 mA cm^{-2}), which was much lower than those of Cu-MoO_2 (−450 mV) and Cu-Mo_2C/CLCN (−231 mV), implying the catalytic activity was regulated by the crystal phase and porous structure. The electrochemically active area of Mo_2C/CLCN (0.7 mF cm^{-2}) was 11–16 times larger than that of Cu-MoO_2 (0.04 mF cm^{-2}) and Cu-Mo_2C/CLCN (0.06 mF cm^{-2}) as shown in Fig. 4**b** and Fig. S12, indicating more available active sites for porous Mo_2C/CLCN. Besides, the HER performance was also better than those of Mo_2C-S1 (−175 mV), and Mo_2C-S2 (−337 mV), implying the shaped rod structure and the exposed Mo catalytic sites protected by Cu were beneficial to the enhanced catalytic activity. As shown in Scheme 2, Cu atoms in the Cu-MoO_2 protected neighboring Mo atoms from being covered by carbon. After removing Cu, the Mo catalytic sites in Mo_2C were exposed. However, the η_{10} value (145 mV) of Mo_2C/CLCN required to arrive at the current density of 10 mA cm^{-2} was still poorer than that (33 mV) of commercial 20 wt% Pt/C.

The corresponding Tafel plots of electrocatalysts were presented in Fig. 4**c**. Although still larger than the Tafel slope of 31.2 mV dec^{-1} of 20 wt% Pt/C, the Tafel slope of 48.2 mV dec^{-1} for Mo_2C/CLCN was much smaller than those of Cu-Mo_2C/CLCN (140.5 mV/dec), Cu-MoO_2 (90 mV dec^{-1}), Mo_2C-S1 (76 mV dec^{-1}), and Mo_2C-S2 (218.7 mV dec^{-1}), demonstrating a faster kinetic HER. The HER inherent activities of these catalysts were assessed by the exchange current density (j_0) based on the Tafel plots. Remarkably, Mo_2C/CLCN exhibited a high j_0 value of 0.062 mA cm^{-2}, and outperformed those of Cu-MoO_2 (2.5×10^{-6} mA cm^{-2}), Cu-Mo_2C/CLCN (3.0×10^{-3} mA cm^{-2}), Mo_2C-S1 (4.3×10^{-3} mA cm^{-2}), and Mo_2C-S2 (0.025 mA cm^{-2}), as shown in Fig. S13. The Nyquist plots and its equivalent circuit of Mo_2C/CLCN modified electrodes were shown in Fig. 4**d**. The charge transfer resistance (Rct) is associated to its electrocatalytic kinetics and low numerical value consistent with the quicker reaction rate, which can be obtained from the semicircle in the high-frequency zone. Rct value of Mo_2C/CLCN was measured to decrease significantly with swelling overpotentials, from ~ 118 Ω at 230 mV to ~ 44 Ω at 290 mV, signifying the quick electron transfer and the advantageous HER kinetics towards the electrolyte interface. In addition, Rct value of Mo_2C/CLCN at 270 mV was much lower than those of Cu-MoO_2, Cu-Mo_2C/CLCN, Mo_2C-S1, Mo_2C-S2, implying the high conductivity and porous structure of CLCN and low HER kinetics, as shown in Fig. S14.

The component of Mo_2C/CLCN, including Cu and Mo_2C, can be regulated by the concentration and etching time of $FeCl_3$ together with ultrasonic treatment. As shown in XRD (Fig. 5**a**) and XPS (Fig. 5**b and c**) results, the Cu were gradually removed by 0.01 M $FeCl_3$ aqueous solution with increased etching time from 10 min, 40–80 min, until no Cu residues were detected. In addition, Mo content maintained unchanged with increased etching time, implying the low concentration of $FeCl_3$ (0.01 M) cannot remove Mo_2C. However, the high concentration of $FeCl_3$ (3 M) combined with ultrasonic treatment can remove both Mo_2C and Cu to obtain pure porous carbon of CLCN. On the basis of the content of carbon in Mo_2C/CLCN, the contents of Cu and Mo elements changed with increased etching time were summarized in Fig. 5**d.** The according morphologies of samples were observed by SEM, and showing that the porous structure gradually appeared by removing Cu and Mo_2C (Fig. S15).

The polarization curves of Mo_2C/CLCN with increasing etching time were shown in Fig. 5**e**, and the according catalytic activities toward HER were dramatically improved. The η_{10} value of Mo_2C/CLCN-10, Mo_2C/CLCN-40 and Mo_2C/CLCN-80 were decreased from 450 mV, 235 mV to 145 mV. The etching time of 80 min was long enough to remove all Cu to obtain pure Mo_2C/CLCN. The longer etching time of 120 min obtained the same component with Mo_2C/CLCN-80 min (Fig. S16), which also possessed the similar HER performance (Fig. S17). The CLCN without Cu and Mo_2C obtained by 3 M $FeCl_3$ etching (80 min) combined with ultrasonic treatment possessed poor HER activity with η_{10} value of 499 mV. CLCN without anchored Mo_2C has negligible electrocatalytic activity, which indicates the robust structure formed by Mo_2C and CLCN reduces the energy input needed to activate HER. Moreover, the electrochemically active area gradually increased with etching time, from 0.09 mF cm^{-2} of Mo_2C/CLCN-10, 0.44 mF cm^{-2} of Mo_2C/CLCN-40 to 0.67 mF cm^{-2} of Mo_2C/CLCN-80 (Fig. 5**f,** Fig. S18). The CLCN possessed the largest electrochemical area of 2.8 mF cm^{-2}, implying porous structure. Therefore, the component and enhanced HER activity of Mo_2C/CLCN can be controlled by $FeCl_3$ etching.

Long-cycle durability of the HER catalyst is of vital significance in practical applications, which are measured by accelerated degradation testing. The i-t testing of Mo_2C/CLCN showed a catalytic current of about 10 mA cm^{-2} remained for over 12 h with no decay at a fixed potential of 150 mV in 0.5 M H_2SO_4 (Fig. 4**e**). As shown in Fig. 4**f**, the cathodic current density showed almost no change in the polarization curves of continuous operation before and after i-t testing. In addition, in order to confirm the practical application, the large current density of 20 mA cm^{-2} and 50 mA cm^{-2} remained for 12 h with no obvious

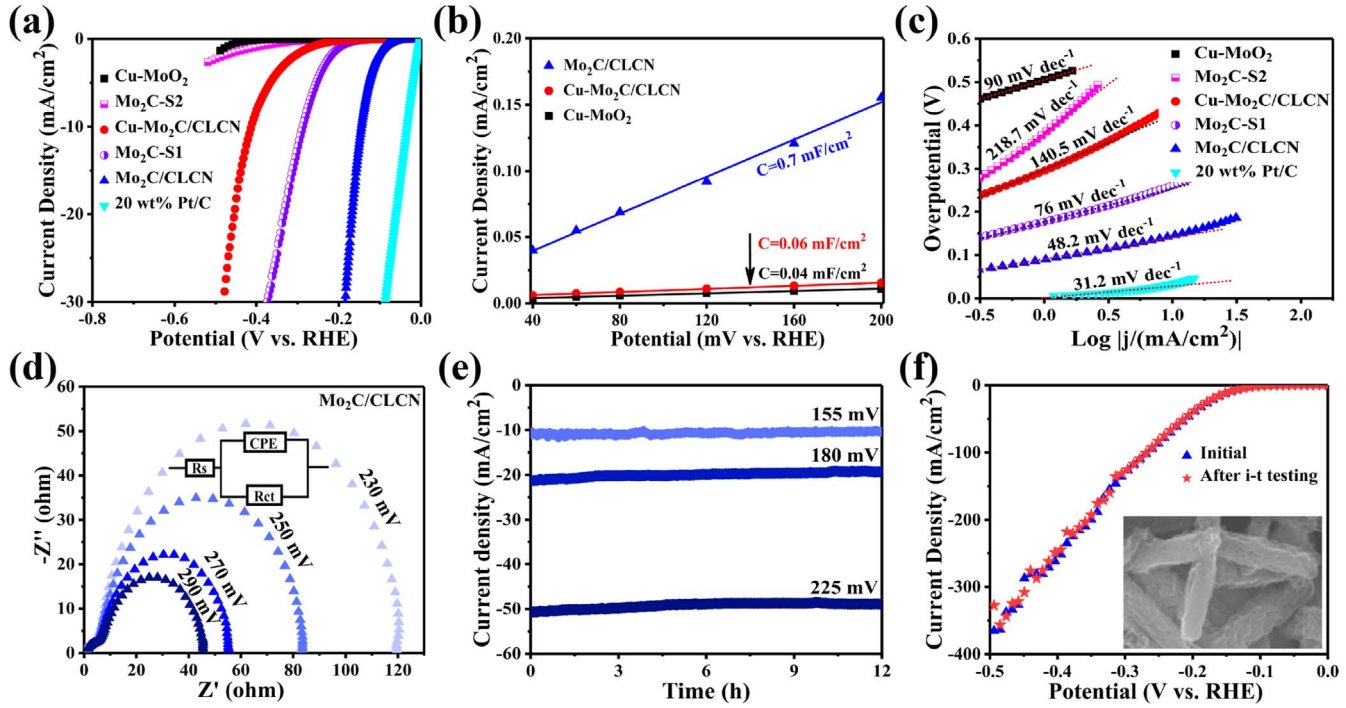

Fig. 4. (a) Polarization curves of Cu-MoO_2, Cu-Mo_2C/CLCN, Mo_2C/CLCN, Mo_2C-S1, Mo_2C-S2 and 20 wt% Pt/C; (b) Distinction of double-layer charging currents at + 0.05 V with various scan rates; (c) Corresponding Tafel plots processed from (a); (d) Nyquist plots of Mo_2C/CLCN at varied overpotentials; (e) Current-time plots with different overpotentials of 155 mV, 180 mV and 225 mV; (f) HER polarization curves for Mo_2C/CLCN before and after i-t testing. Inset is the SEM image of Mo_2C/CLCN after i-t testing.

attenuation (Fig. 4**e**). The gathered bubbles on Mo_2C/CLCN modified electrode were authenticated to be H_2 by gas chromatography, and the corresponding hydrogen production rate was 6.5 mmol mg^{-1} h^{-1} with faradic efficiency of ~ 98%, as shown in Fig. S19. In addition, no significant changes of morphology (inset of Fig. 4**f**) and crystalline phase (XRD, Fig. S20) confirmed the structural integrity as well as catalytic stability of Mo_2C/CLCN. Furthermore, Mo_2C/CLCN had a highly competent HER performance over a broad pH range, from 0.5 M H_2SO_4 (pH 0.25), 1 M phosphate buffer solution (pH 7) to 1 M KOH (pH 14), which were confirmed by polarization curves (Fig. S21a and S21b) and current-time plots (Fig. S21c).

All these results indicated that Mo_2C/CLCN was an excellent active material for Mo-based HER catalysts and displayed excellent electrochemical properties. The Cu-MoO_2 rods as Mo source and Cu template

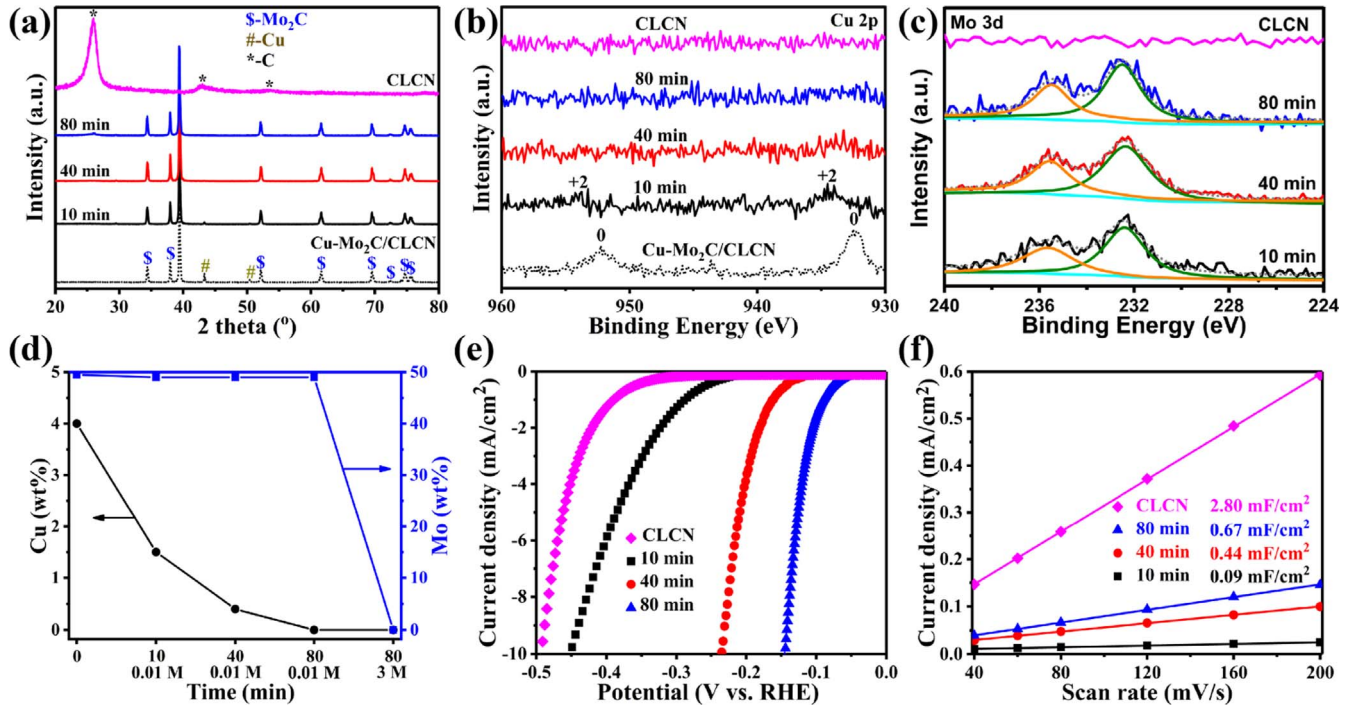

Fig. 5. (a) XRD patterns; XPS spectra of (b) Cu 2p and (c) Mo 3d; (d) the contents of Cu and Mo with changing etching time; (e) polarization curves and (f) electrochemical surface area of Mo_2C/CLCN etched by 0.01 M $FeCl_3$ for 10 min, 40 min, 80 min and CLCN obtained by 3 M $FeCl_3$ etching (80 min) combined with ultrasonic treatment.

played the significant and multifunctional effect on enhancing the HER activity of Mo_2C/CLCN. First, the Cu regulated the morphology to obtain the Cu-MoO_2 rod structure as precursor; Second, the Cu catalytically synthesized the graphene sheets to form cross-linked carbon network, and then removing Cu to form porous carbon structure; Third, the steric protection of Cu limited the particle size of Mo_2C even at a high calcination temperature of 1000 °C; Fourth, the Cu protected Mo_2C from covering excess carbon during carbonation and exposed Mo_2C by removing Cu. So, the excellent HER performance was due to the 3D porous carbon structure and exposed Mo_2C, which were regulated by Cu. Strikingly, the Mo_2C/CLCN possessed the integrated HER performance with onset potential of −85 mV, Tafel value of 48.2 mV dec^{-1} and low overpotential (145 mV at 10 mA cm^{-2}) with a large exchange current density (0.062 mA cm^{-2}), which performed superior or close to most of the documented non-noble-metal catalysts in acidic electrolytes, such as Mo_2C/CNT (Tafel value of 65 mV dec^{-1} and overpotential of 152 mV at 10 mA cm^{-2}) [40], Mo_2C/GCSs (onset potential of −120 mV, Tafel value of 62.6 mV dec^{-1} and overpotential of 200 mV at 10 mA cm^{-2}) [41], β-Mo_2C nanotubes (onset potential of −82 mV, Tafel value of 58 mV dec^{-1} and overpotential of 136 mV at 10 mA cm^{-2}) [20], Mo_2C nanowires (onset potential of −70 mV, Tafel value of ~ 53 mV dec^{-1} and overpotential of ~ 200 mV at 10 mA cm^{-2}) [18], MoC_x nano-octahedrons (onset potential of −87 mV, Tafel value of 53 mV dec^{-1} and overpotential of 142 mV at 10 mA cm^{-2}, exchange current density of 0.023 mA cm^{-2}) [13], Mo_2C/CNT-graphene (onset potential of −62 mV, Tafel value of 62 mV dec^{-1} and low overpotential of 172 mV at 10 mA cm^{-2}) [42], Mo_2C@NC (onset potential of −60 mV, Tafel value of 60 mV dec^{-1} and overpotential of 124 mV at 10 mA cm^{-2}) [21], Mo_2C (onset potential of −105 mV, Tafel value of 70 mV dec^{-1} and overpotential of 192 mV at 10 mA cm^{-2}) [26], Mo_2C-C (onset potential of −100 mV, Tafel value of 85 mV dec^{-1} and overpotential of 164 mV at 10 mA cm^{-2}) [24] (Table S2).

4. Conclusions

In summary, we have reported that Mo_2C on hierarchical porous carbon rods composed of cross-linked carbon networks (Mo_2C/CLCN) were synthesized by using Cu-MoO_2 rods as Mo source and Cu template. DFT calculation confirmed Mo atoms on C plane were the main catalytic sites of Mo_2C but the residual C atoms covered Mo atoms reduced catalytic activities of Mo_2C. This strategy presented significance in the formation of hierarchical porous carbon to increase electrochemical active area and exposure of Mo_2C toward efficient HER. Profiting from the unique nanostructure, the Mo_2C/CLCN demonstrated noteworthy electrocatalytic activity toward HER in all pH values with robust stability. The Mo_2C/CLCN possessed the high HER catalytic activity, including η_0 of −85 mV, η_{10} of 145 mV, Tafel slope of 48.2 mV dec^{-1} and robust stability in 0.5 M H_2SO_4. Moreover, such a synthetic stratagem may well make great efforts for the better popularization and application to manufacture nano/microstructured framework of Mo_2C, thus paving the way for developing improved performance functional materials for various applications.

Acknowledgements

This work was supported by Project of Public Interest Research and Capacity Building of Guangdong Province (2014A010106005), Guangdong Innovative and Entrepreneurial Research Team Program (2014ZT05N200), Tip-top Scientific and Technical Innovative Youth Talents of Guangdong Special Support Program (2016TQ03N541), Guangdong Natural Science Funds for Distinguished Young Scholar (2017A030233174) and the National Natural Science Foundation of China (51502096).

Appendix A. Supporting information

Supplementary data associated with this article can be found in the online version at http://dx.doi.org/10.1016/j.nanoen.2017.10.030.

References

[1] Y. Jiao, Y. Zheng, M. Jaroniec, S.Z. Qiao, Chem. Soc. Rev. 44 (2015) 2060–2086.
[2] X. Zou, Y. Zhang, Chem. Soc. Rev. 44 (2015) 5148–5180.
[3] X. Cao, C. Tan, M. Sindoro, H. Zhang, Chem. Soc. Rev. 46 (2017) 2660–2677.
[4] X. Cao, C. Tan, X. Zhang, W. Zhao, H. Zhang, Adv. Mater. 28 (2016) 6167–6196.
[5] W. Zhou, T. Xiong, C. Shi, J. Zhou, K. Zhou, N. Zhu, L. Li, Z. Tang, S. Chen, Angew. Chem. Int. Ed. 55 (2016) 8416–8420.
[6] L. Zhang, S. Yu, J. Zhang, J. Gong, Chem. Sci. 7 (2016) 3500–3505.
[7] L. Zhu, H. Lin, Y. Li, F. Liao, Y. Lifshitz, M. Sheng, S.-T. Lee, M. Shao, Nat. Commun. 7 (2016) 12272.
[8] Y. Zheng, Y. Jiao, Y. Zhu, L.H. Li, Y. Han, Y. Chen, A. Du, M. Jaroniec, S.Z. Qiao, Nat. Commun. 5 (2014) 3783.
[9] W.J. Zhou, J. Jia, J. Lu, L.J. Yang, D.M. Hou, G.Q. Li, S.W. Chen, Nano Energy 28 (2016) 29–43.
[10] J. Wang, W. Cui, Q. Liu, Z. Xing, A.M. Asiri, X. Sun, Adv. Mater. 28 (2016) 215–230.
[11] Y. Shi, B. Zhang, Chem. Soc. Rev. 45 (2016) 1529–1541.
[12] J. Wang, F. Xu, H. Jin, Y. Chen, Y. Wang, Adv. Mater. 29 (2017) 1605838.
[13] H.B. Wu, B.Y. Xia, L. Yu, X.Y. Yu, X.W. Lou, Nat. Commun. 6 (2015) 6512.
[14] J. Chen, W. Zhou, J. Jia, B. Wan, J. Lu, T. Xiong, Q. Tong, S. Chen, Int. J. Hydrog. Energy 42 (2017) 6448–6454.
[15] X. Fan, H. Zhou, X. Guo, ACS Nano 9 (2015) 5125–5134.
[16] D.V. Esposito, S.T. Hunt, Y.C. Kimmel, J.G. Chen, J. Am. Chem. Soc. 134 (2012) 3025–3033.
[17] W.F. Chen, S. Iyer, S. Iyer, K. Sasaki, C.H. Wang, Y.M. Zhu, J.T. Muckerman, E. Fujita, Energy Environ. Sci. 6 (2013) 1818–1826.
[18] L. Liao, S. Wang, J. Xiao, X. Bian, Y. Zhang, M.D. Scanlon, X. Hu, Y. Tang, B. Liu, H.H. Girault, Energy Environ. Sci. 7 (2014) 387–392.
[19] L. Chen, H. Jiang, H. Jiang, H. Zhang, S. Guo, Y. Hu, C. Li, Adv. Energy Mater. (2017) 1602782.
[20] F.X. Ma, H.B. Wu, B.Y. Xia, C.Y. Xu, X.W. Lou, Angew. Chem. Int. Ed. 54 (2015) 15395–15399.
[21] Y. Liu, G. Yu, G.D. Li, Y. Sun, T. Asefa, W. Chen, X. Zou, Angew. Chem. Int. Ed. 54 (2015) 10752–10757.
[22] H. Vrubel, X. Hu, Angew. Chem. Int. Ed. 124 (2012) 12875–12878.
[23] J. Jia, W. Zhou, G. Li, L. Yang, Z. Wei, L. Cao, Y. Wu, K. Zhou, S. Chen, ACS Appl. Mater. Interfaces 9 (2017) 8041–8046.
[24] Z. Wu, J. Wang, R. Liu, K. Xia, C. Xuan, J. Guo, W. Lei, D. Wang, Nano Energy 32 (2017) 511–519.
[25] R. Ma, Y. Zhou, Y. Chen, P. Li, Q. Liu, J. Wang, Angew. Chem. Int. Ed. 54 (2015) 14723–14727.
[26] Z.Y. Wu, B.C. Hu, P. Wu, H.W. Liang, Z.L. Yu, Y. Lin, Y.R. Zheng, Z.Y. Li, S.H. Yu, NPG Asia Mater. 8 (2016) e288.
[27] Y. Huang, Q. Gong, X. Song, K. Feng, K. Nie, F. Zhao, Y. Wang, M. Zeng, J. Zhong, Y. Li, ACS Nano 10 (2016) 11337–11343.
[28] Q. Gong, Y. Wang, Q. Hu, J. Zhou, R. Feng, P.N. Duchesne, P. Zhang, F. Chen, N. Han, Y. Li, C. Jin, Y. Li, S.T. Lee, Nat. Commun. 7 (2016) 13216.
[29] S.T. Hunt, T. Nimmanwudipong, Y. Román-Leshkov, Angew. Chem. Int. Ed. 53 (2014) 5131–5136.
[30] G. Kresse, J. Hafner, Phys. Rev. B 48 (1993) 13115.
[31] G. Kresse, J. Furthmüller, Comp. Mater. Sci. 6 (1996) 15–50.
[32] P.E. Blöchl, Phys. Rev. B 50 (1994) 17953.
[33] J.P. Perdew, K. Burke, M. Ernzerhof, Phys. Rev. Lett. 77 (1996) 3865.
[34] J.K. Nørskov, T. Bligaard, A. Logadottir, J. Kitchin, J.G. Chen, S. Pandelov, U. Stimming, J. Electrochem. Soc. 152 (2005) J23–J26.
[35] L. Yang, W. Zhou, D. Hou, K. Zhou, G. Li, Z. Tang, L. Li, S. Chen, Nanoscale 7 (2015) 5203–5208.
[36] W. Zhou, D. Hou, Y. Sang, S. Yao, J. Zhou, G. Li, L. Li, H. Liu, S. Chen, J. Mater. Chem. A 2 (2014) 11358–11364.
[37] M. Xiang, D. Li, W. Li, B. Zhong, Y. Sun, Catal. Commun. 8 (2007) 513–518.
[38] J.A. Schaidle, A.C. Lausche, L.T. Thompson, J. Catal. 272 (2010) 235–245.
[39] P.R. Kidambi, B.C. Bayer, R. Blume, Z.-J. Wang, C. Baehtz, R.S. Weatherup, M.-G. Willinger, R. Schloegl, S. Hofmann, Nano Lett. 13 (2013) 4769–4778.
[40] W.F. Chen, C.H. Wang, K. Sasaki, N. Marinkovic, W. Xu, J.T. Muckerman, Y. Zhu, R.R. Adzic, Energy Environ. Sci. 6 (2013) 943–951.
[41] W. Cui, N. Cheng, Q. Liu, C. Ge, A.M. Asiri, X. Sun, ACS Catal. 4 (2014) 2658–2661.
[42] D.H. Youn, S. Han, J.Y. Kim, J.Y. Kim, H. Park, S.H. Choi, J.S. Lee, ACS Nano 8 (2014) 5164–5173.

Jin Jia received his Bachelor's degree (2012) and Master's degree (2015) in materials science and engineering from Henan Polytechnic University (HPU). He is currently pursuing Ph.D. degree under the supervision of Prof. Weijia Zhou and Prof. Shaowei Chen in the School of Environment and Energy at the South China University of Technology (SCUT). His current research interest focuses on the design and synthesis of nanomaterials for energy conversion and storage.

Dr. Weijia Zhou completed his Ph.D. at Shandong University in 2012. He was doing research at Nanyang Technological University (NTU) in 2011. Now, Dr. Zhou is an associate professor of New Energy Research Institute, School of Environment and Energy, South China University of Technology (SCUT), China. His research interests are related to the design and synthesis of functional materials and devices for new energy conversion and storage, including photo and electro-catalytic water splitting and supercapacitor.

Zhaoqian Wei received B.S. degree from Guizhou University of Technology in 2016. She is pursuing her M.D. degree under the supervision of Prof. Weijia Zhou and Prof. Shaowei Chen in New Energy Research Institute, South China University of Technology (SCUT). Her research interests include electrocatalytic water splitting and CO_2 reduction.

Tanli Xiong achieved his B.S. Degree from School of Environmental Science and Engineering, Hubei University of Technology in 2015, and now is currently pursuing his Master Degree under the supervision of Prof. Weijia Zhou in the school of Environment and Energy at South China University of Technology, China. His research is focused on the simulation of nanomaterials as electrocatalyst for hydrogen evolution reaction.

Guixiang Li obtained his B.S. Degree from School of Environmental Science and Engineering, Kunming University of Science and Technology in 2016, and now is currently pursuing his Master Degree under the supervision of Prof. Weijia Zhou in the school of Environment and Energy at South China University of Technology, China. His research is focused on the synthesis of nanomaterials as electrocatalyst for hydrogen evolution reaction and electrochemical water treatment.

Lili Zhao obtained B.S. degrees at Shandong University in China in 2013. Now, she studies as a Ph.D. student in Prof. Hong Liu's group in State Key Laboratory of Crystal Materials, Shandong University, China since September 2013. Her research interests are properties of piezoelectric and ferroelectric nanomaterials, catalysts for photocatalytic and electrochemical water splitting.

Xiaofei Zhang obtained his B.E. degree from Shandong University in 2015. Currently, he studies as a master student in Prof. Hong Liu's group in State Key Laboratory of Crystal Materials, Shandong University, China since September 2015. His research interests are synthesis of nanomaterials and their application in energy area, including photocatalysis, solar thermal and solar electricity generation.

Dr. Hong Liu is a professor in State Key Laboratory of Crystal Materials, Shandong University. He received his Ph.D. degree in 2001 from Shandong University (China). His current research is mainly focused on chemical processing of nanomaterials for energy related applications including photocatalysis, tissue engineering, especially the interaction between stem cell and nanostructure of biomaterials, as well as the nonlinear optical crystals.

Dr. Jian Zhou is an associate professor in the department of materials science and engineering of Nanjing University, China. He received his Ph.D. degree in 2007 from department of physics of Nanjing University. His current research interest is the first principles calculation for electronic, magnetic, optical and topological properties of the layered or two-dimensional materials.

Dr. Shaowei Chen obtained a B.Sc. degree from the University of Science and Technology of China, and then went to Cornell University receiving his M.Sc. and Ph.D. degrees in 1993 and 1996. Following a postdoctoral appointment in the University of North Carolina at Chapel Hill, he started his independent career in Southern Illinois University in 1998. In 2004, he moved to the University of California at Santa Cruz and is currently a Professor of Chemistry. He is also an adjunct professor at South China University of Technology. His research interest is primarily in the electron transfer chemistry of nanoparticle materials.